AIP | Physics of Fluids

Comparison of very-large-scale motions of turbulent pipe and boundary layer simulations

Jae Hwa Lee and Hyung Jin Sung

Citation: Phys. Fluids **25**, 045103 (2013); doi: 10.1063/1.4802048
View online: http://dx.doi.org/10.1063/1.4802048
View Table of Contents: http://pof.aip.org/resource/1/PHFLE6/v25/i4
Published by the AIP Publishing LLC.

PHYSICS OF FLUIDS **25**, 045103 (2013)

Comparison of very-large-scale motions of turbulent pipe and boundary layer simulations

Jae Hwa Lee and Hyung Jin Sung[a)]
Department of Mechanical Engineering, KAIST 291 Daehak-ro, Yuseong-gu, Daejeon 305-701, South Korea

(Received 28 August 2012; accepted 1 April 2013; published online 29 April 2013)

A direct numerical simulation of a fully developed turbulent pipe flow was performed to investigate the similarities and differences of very-large-scale motions (VLSMs) to those of turbulent boundary layer (TBL) flows. The Reynolds number was set to $Re_D = 35\,000$, and the computational domain was 30 pipe radii in length. Inspection of instantaneous fields, streamwise two-point correlations, and population trends of the momentum regions showed that the streamwise length of the structures in the pipe flow grew continuously beyond the log layer ($y/\delta < 0.3$–0.4) with a large population of long structures ($>3\delta$), and the maximum length of the VLSMs increased up to $\sim 30\delta$. Such differences between the TBL and pipe flows arose due to the entrainment of large plumes of the intermittent potential flow in the TBL, creating break-down of the streamwise coherence of the structures above the log layer with the strong swirling strength and Reynolds shear stress. The average streamwise length scale of the pipe flow was approximately 1.5–3.0 times larger than that of the TBL through the log and wake regions. The maximum contribution of the structures to the Reynolds shear stress was observed at approximately 6δ in length, whereas that of the TBL was at 1δ–2δ, indicating a higher contribution of the VLSMs to the Reynolds shear stress in the pipe flow than in the TBL flow. © *2013 AIP Publishing LLC*. [http://dx.doi.org/10.1063/1.4802048]

I. INTRODUCTION

Experimental and numerical studies have shown that long structures in the logarithmic layer play a crucial role in the turbulent boundary layer (TBL). These structures correspond to bulges or hairpin packets of large-scale motions (LSMs) with streamwise extents on the order of 2δ–3δ (δ is the outer length scale) and the very-large-scale motions (VLSMs) or "superstructures" with the sizes in the range of 10δ–50δ.[1–7] Adrian[8] and Marusic *et al.*[9] provided excellent reviews of these interesting structures. Hairpin packets consist of a coherent group of hairpin vortices aligned along the streamwise direction. The structures contribute 25% of the Reynolds shear stress while occupying less than 4.5% of the total area.[2] On the other hand, the spatial features of the very-large-scale structures form very long meandering positive and negative streamwise velocity fluctuations. Hutchins and Marusic[4] showed that these structures have a streamwise length of $O(20\delta)$, while Dennis and Nickels[7] reported that nearly all VLSMs are found to be below 7δ in the TBL. In a very recent direct numerical simulation (DNS) study, Lee and Sung[5] found that the momentum regions in the log layer with lengths greater than 3δ–4δ accounted for more than 40% of all patches with the maximum length $\sim 18\delta$, and these VLSMs contributed to approximately 45% of the total Reynolds shear stress with strong swirling motions.

In addition to their presence in the log and wake regions of TBLs, VLSMs have been observed in pipe and channel flows, with some structural differences.[10,11] Monty *et al.*[10] examined the

a)Author to whom correspondence to be addressed. Electronic mail: hjsung@kaist.ac.kr. Tel.: 82-42-350-3027. Fax: 82-42-350-5027.

structures of fully developed turbulent pipe and channel flows using hot-wire probes according to Taylor's hypothesis, which converts temporal experimental measurements into a spatial domain. They showed that very long meandering structures up to 25 channel half-heights in length existed in the logarithmic layer of the channel flow, and these structures persisted at least until $y/\delta = 0.56$. However, the use of Taylor's hypothesis raises concerns in wall-bounded flows because the accuracy of Taylor's hypothesis decreases as the apparent structure size increases. Dennis and Nickels[12] showed that the linear fit of the correlation between the Taylor field and its corresponding spatial field drops to zero at $x/\delta = 9.32$, indicating large inaccuracy in examining VLSMs by Taylor's hypothesis. A good example is seen in the inconsistent maximum streamwise extent induced by the Taylor fields: the order of 20δ and 7δ in the TBLs by Hutchins and Marusic[4] and Dennis and Nickels,[7] respectively. Therefore, true spatial field based on DNS is valuable to show the precise information of VLSMs. In aspects of statistical properties of the VLSMs, Monty *et al.*[10] and Bailey *et al.*[11] showed that the spanwise width scales of the pipe and channel flows were approximately twice larger than that observed in the logarithmic layer of the TBL. In their studies, however, streamwise information was lacking due to experimental difficulties associated with measuring the streamwise extents of structures that were very long with the order of 8δ–16δ in turbulent pipe flows.[13,14]

Prior to observing the spatial fields of VLSMs, the existence of VLSMs was hinted in the premultiplied one-dimensional spectra associated with the streamwise velocity fluctuations.[3,13–16] Kim and Adrian[13] examined the premultiplied spectra of a turbulent pipe flow at $y^+ = 132$ and interpreted the spectral envelope as a bi-modal distribution with maxima that indicated wavelengths associated with VLSMs and LSMs. However, the experimental results based on energy spectra showed that the maximum wavelength from the secondary energy peak indicating the VLSM was scattered across 10δ–50δ and that the wall-normal height at which the maximum wavelengths of VLSMs occur was not determined consistently among the experiments,[14,15,17] although the Reynolds number was very similar. Furthermore, the energy spectra of all experimental results were obtained based on Taylor's approximation. Since applying Taylor's hypothesis was observed not only to shift energy in very long wavelengths to shorter wavelengths but also to modify the shape of the spectrum, this gives rise to an artificial secondary peak.[18] This issue has also been raised by Wu *et al.*[19] and Kim.[20] Kim[20] reported that since the detection of VLSMs are mostly based on Taylor's hypothesis, it is not sure whether the VLSMs are real, or experimental or numerical artifact. With the debate on the existence of the secondary peak in the energy spectrum, therefore, previous spatial information derived by artificial secondary peak is not complete.

In the present study, a DNS of a fully developed turbulent pipe flow at $Re_\tau = 934$ was conducted to investigate the spatially coherent structures of VLSMs with a 30 pipe radii long streamwise domain in length, particularly in comparison with the structures observed in the TBL. VLSMs may be influenced by a variety of factors, including the experimental conditions, measurement methods, Reynolds number, numerical conditions of the simulation, computational box, and grid resolution. In the current work, therefore, we employed our numerical code that was used to simulate a TBL under similar Reynolds number conditions. We analyzed the DNS data from the pipe flows in comparison with the boundary layer data presented by Lee and Sung[21] at $Re_\tau = 850$. The Reynolds numbers of the present study and the study described in Lee and Sung[21] are not significantly different, and thus the main conclusions regarding the spatial features of the turbulent structures are relatively insensitive to such small differences. The structure of the paper is as follows: The numerical code and simulation details are introduced in Sec. II, and the turbulent statistics are briefly discussed in Sec. III. The instantaneous and statistical analysis results are discussed in Secs. IV and V, followed in Sec. IV by the results of the population trends in the momentum regions. Finally, the paper provides a summary and conclusions.

II. NUMERICAL METHOD

For an incompressible, fully developed turbulent flow over a smooth wall, the Navier-Stokes and continuity equations in cylindrical coordinates were employed as governing equations. Here, the notation r is the radial coordinate measured along the pipe axis, z is the flow axial direction,

and θ is the azimuthal coordinate, and u_r, u_z, u_θ are the corresponding velocity components. The maximum velocity of the fully developed laminar profile (U_c) and the pipe radius (R) were used to non-dimensionalize the equations. The unit time scale is given as R/U_c and the Reynolds number based on the pipe diameter (D) and bulk velocity (U_b) is $Re_D = 35\,000$.

The governing equations were integrated in time using the fractional step method along with the implicit velocity decoupling procedure.[22] A block LU decomposition based on approximate factorization was applied to achieve both velocity-pressure decoupling and the decoupling of intermediate velocity components. In this approach, the terms were first discretized in time using the Crank-Nicholson method, and then the coupled velocity components were solved without iteration. All terms were resolved using a second-order central difference scheme in space with a staggered mesh. No-slip conditions were applied to the velocities at the wall. Periodic boundary conditions were applied along the streamwise and azimuthal directions. The centerline condition for the radial velocity was obtained by averaging the corresponding values across the centerline.[23] The derivatives of the quantities staggered with respect to the centerline were obtained by differencing opposing values across the centerline, accounting for reversals in the directions of the radial and azimuthal unit vector through the centerline. Further numerical details may be found in Refs. 22 and 24.

The streamwise domain adopted here was 30 pipe radii, because the previous experimental studies of Kim and Adrian[13] suggested the existence of VLSMs with mean wavelengths of up to 8δ–16δ based on the premultiplied spectra in high Reynolds number pipe flows. In addition, a recent DNS study by Chin *et al.*[25] indicated that the required pipe length for the convergence of all turbulence statistics in the outer regions was 8π pipe radii at $Re_\tau = 170$ and 500. Note that the longest streamwise domain reported previously under similar or higher Reynolds number conditions was 15 pipe radii in a turbulent pipe flow.[26] Recently, longer domains were used in DNS studies of turbulent pipe flows by Chin *et al.*[25] and Wu *et al.*,[19] although the Reynolds numbers were smaller than in the present study.

The finite-difference grid size employed in the current work was $4097 \times 301 \times 1025$ along the axial, radial, and azimuthal directions, respectively. The grid resolutions are shown in Table I. The grid distribution along the wall-normal direction was the same as that reported in Ref. 26. Hence, the minimum and maximum spacing at $r = R$ and $0.406R$ were 0.334 and 9.244 in the wall units, respectively. The velocity field was initialized using a laminar mean velocity profile, and random fluctuations were superimposed with a maximum amplitude of 30% of the maximum velocity U_c. During the first 400 iterations, the maximum axial CFL component was fixed at a small value of 0.1, and the corresponding time step was 0.0004. These conditions equilibrated out the unrealistic effects associated with the imposed unrealistic initial velocity field. After the first 400 iterations, the computational time step was fixed at $\Delta t = 0.01$, and the maximum CFL component in the axial direction was set to 1.25. The simulation was run initially for $32\,000R/U_c$ in order to eliminate transient processes, and the statistics were sampled during last $174\,000R/U_c$ steps using 64 parallel processors (IBM p595) at the KISTI supercomputer center. The sampling time duration was $1740R/U_c$, sufficient to allow particles to travel through the pipe axial dimensions at the bulk velocity more than 25 times.

To facilitate a comparison with the coordinates of the boundary layer, we defined the axial coordinate as $x = z$, the wall-normal coordinate $y = 1 - r$, and the spanwise coordinate $z = r\theta$. This arc length was discussed in Refs. 10 and 19. In addition, it is helpful to introduce the analogous velocity components $u = u_z$, $v = -u_r$, and $w = u_\theta$. Finally, in the present study, the superscript $+$ refers to quantities normalized by the friction velocity u_τ, and capital letters depict the temporally and spatially averaged statistics. Since pipe flow is homogeneous in the streamwise and spanwise directions, we denote the horizontal distance as the relative distance r_x and r_x.

TABLE I. Domain size and mesh resolution.

Re_D	Re_τ	L_x/R	N_x, N_y, N_z	Δx^+	$\Delta(R\theta)^+$	$\Delta r^+{}_{min}$	$\Delta r^+{}_{max}$	$\Delta t U_c/R$
35 000	934	30	4097, 301, 1025	6.84	5.73	0.33	9.24	0.01

III. VALIDATION OF DNS RESULTS

Before proceeding further, we present the first- and second-order turbulence statistics with previous numerical pipe data at two Reynolds numbers to establish the validity of our simulation. We also included the results with the DNS TBL data from Schlatter and Örlü.[27] Note that the Reynolds number of Schlatter and Örlü,[27] $Re_\theta = 3030$ ($Re_\tau = 974$), was closer to the Reynolds number of the present pipe flow ($Re_\tau = 934$). Additionally, their boundary layer flow was simulated over a sufficiently long streamwise domain using the fringe method because the features of the TBL developed spatially along the streamwise direction. In Fig. 1, the inner and outer scaled mean velocity profiles of our data showed the excellent agreement with the pipe data from Wu *et al.*[19] and Wu and Moin[26] at $Re_\tau = 685$ and 1142. A comparison of the mean velocity profiles of the pipe with TBL flows showed that in the log region the mean velocity in the TBL has somewhat lower value than in the pipe flow, as shown in the enlarged view. Nagib and Chauhan[28] also exhibited the consistent result that the intercept of the log law profile is higher in the pipe flow. In addition, it is obvious that the profiles of the pipe flow further extended to the outer layer lying closer to the log-law profile far from the wall, even though the Reynolds numbers were similar. This observation was previously described in the experimental study of Monty *et al.*[10] at higher Reynolds numbers. They showed that because very long coherent structures were populated in the log region, a more logarithmic mean velocity indicated the presence of extended streamwise coherence among the structures far from the wall. Differences among the data sets in the outer layers could be explained in terms of the intermittent behavior of the boundary layer because the mean streamwise velocity in the potential region exceeded that in the rotational region.[29]

Figure 2 shows the profiles of the turbulence intensities and the Reynolds shear stress in the outer coordinates. The available streamwise and spanwise intensity profiles of the turbulent pipe flows are included in (a) and (c). The streamwise intensities along with three Reynolds numbers illustrate the Reynolds number dependent behavior on the near-wall peak values in the pipe flow. This dependence agreed with those over the turbulent channel and TBL flows.[9,30] However, hot-wire experiments by Hultmark *et al.*[31] found clear difference of the peak value between the pipe and TBL flows. They showed that the magnitude of the streamwise peak value in the pipe flow was nearly constant for all Reynolds numbers considered in their experiments. In Fig. 2(a), the streamwise intensities for the pipe flow agreed well (to within 2%) with the near-wall behavior of the TBL flow up to $y^+ \sim 40$. Similar to the other components, however, the differences became pronounced at larger wall-normal distances, and a maximum difference was observed at $y/\delta = 0.4$–0.5. Although not shown here, this difference in the streamwise intensity profile was not observed in the comparison of the pipe DNS data at $Re_\tau = 934$ with our boundary layer DNS data at $Re_\tau = 850$ in which the streamwise intensity profiles collapse in the outer layer.

IV. INSTANTANEOUS ANALYSIS

We visualized true spatial fields of the large- and very-large-scale structures in the pipe flow at the wall-normal heights of $y/\delta = 0.15$, 0.3, and 0.5. For turbulent pipe flows, Monty *et al.*[10]

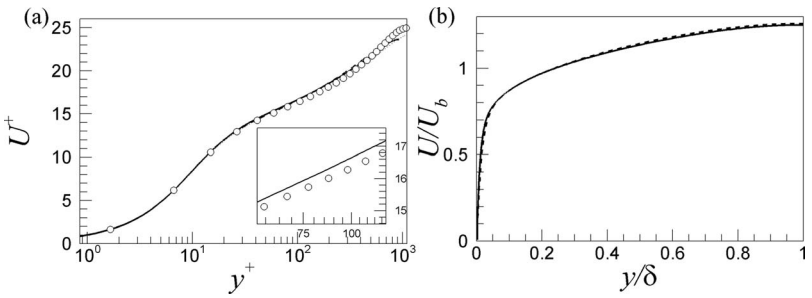

FIG. 1. Mean velocity profiles U^+ in (a) inner and (b) outer coordinates. Solid line: present DNS; dashed line: Wu *et al.*[19] at $Re_D = 24\,580$; dotted line: Wu and Moin[26] at $Re_D = 44\,000$; circles: TBL data, Schlatter and Örlü[27] at $Re_\theta = 3030$.

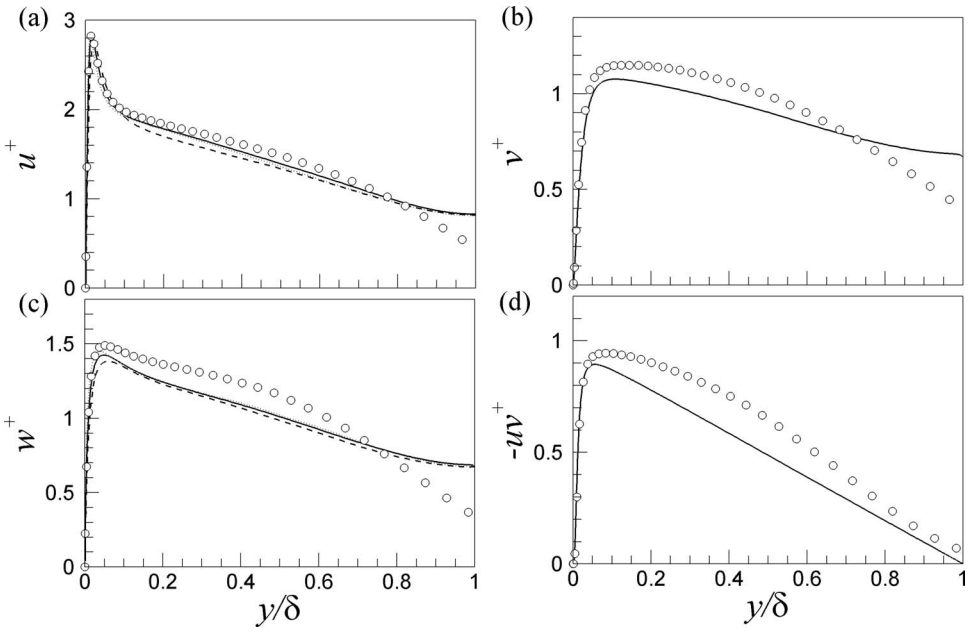

FIG. 2. (a)–(d) Turbulence intensities and Reynolds shear stress along the outer coordinates. The legend is the same as in Fig. 1.

and Hellström *et al.*[32] showed the spatial fields of the streamwise velocity fluctuations constructed using Taylor's hypothesis at the fixed wall-normal locations of $y/\delta = 0.15$ and 0.2, respectively. As mentioned earlier, however, since the accuracy of the Taylor field is decreased with increasing the streamwise distance with large error,[12] it would be worth considering the instantaneous fields based on DNS data without any application of Taylor's hypothesis. Figures 3 and 4 show the very-large-scale low- and high-momentum regions along with the signed 2D swirling strength ($\Lambda_{ci} = \lambda_{ci}\omega_y/|\omega_y|$) and the second- and fourth-quadrant Reynolds shear stresses (Q2 and Q4 events). The black contours indicate low- and high-momentum regions with $u^+ = -0.5$ and 0.5, respectively.

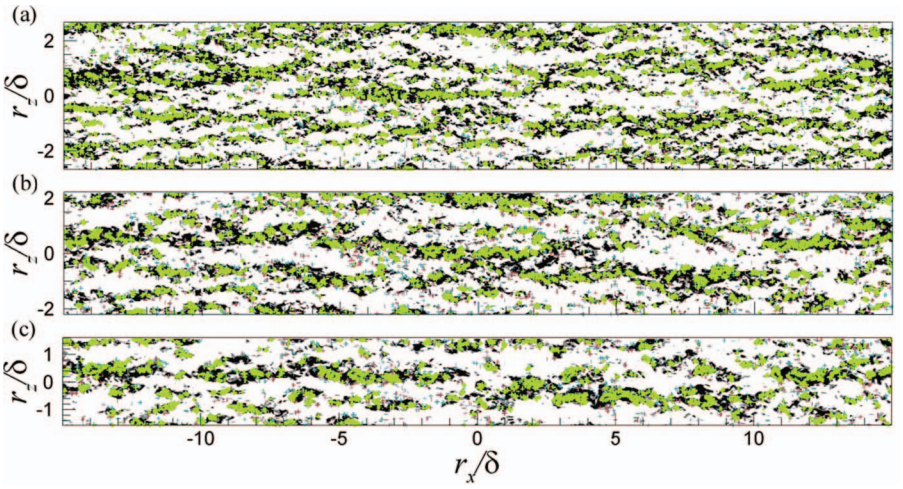

FIG. 3. Very-large-scale low-momentum regions with 2D signed swirling strengths ($\Lambda_{ci} = \lambda_{ci}\omega_y/|\omega_y|$) and second-quadrant Reynolds shear stress (Q2 event). (a) $y/\delta = 0.15$, (b) $y/\delta = 0.3$, and (c) $y/\delta = 0.5$. Blue and red contours indicate the positive and negative values of Λ_{ci} with magnitudes of 30% of the maximum and minimum values. The luminous contours indicate a Q2 event with magnitude $-3\overline{uv}^+$. The flow is from left to right.

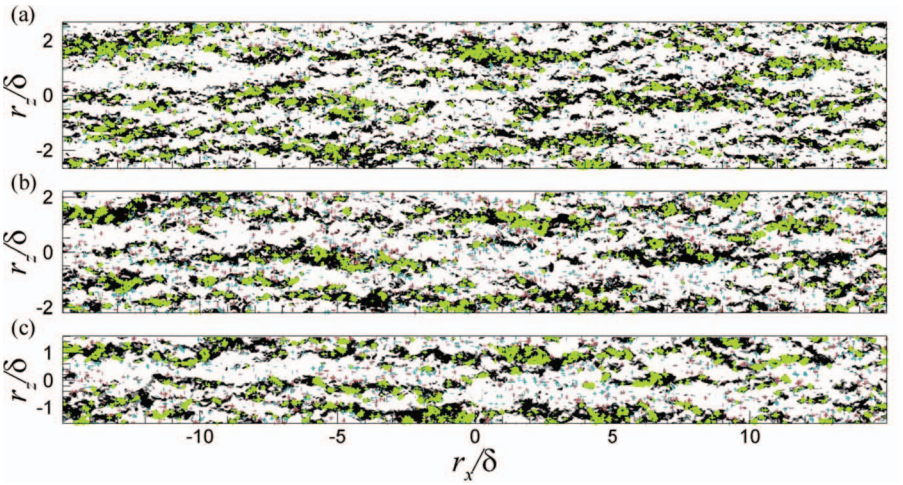

FIG. 4. Very-large-scale high-momentum regions with 2D signed swirling strengths ($\Lambda_{ci} = \lambda_{ci}\omega_y/|\omega_y|$) and fourth-quadrant Reynolds shear stress (Q4 event). (a) $y/\delta = 0.15$, (b) $y/\delta = 0.3$, and (c) $y/\delta = 0.5$. Blue and red contours indicate the positive and negative values of Λ_{ci} with a magnitude of 30% of the maximum and minimum values. The luminous contours indicate a Q4 event with magnitude $-3\overline{uv}^+$.

In order to show the vortex pattern related to the hairpin legs,[33] we present the swirling strength (λ_{ci}) with magnitudes of 30% of the maximum and minimum values and the signed swirling strength ($\Lambda_{ci} = \lambda_{ci}\omega_y/|\omega_y|$) was introduced by multiplying the sign of the vorticity to distinguish the direction of rotation in the xz plane.[34]

Figure 3(a) shows that the large- and very-large-scale streamwise-aligned structures were present in the logarithmic layer, and these structures were closely associated with the strong swirling strength and the Q2 Reynolds shear stress. This suggests that the long structures were created by the coherent alignment of groups of the hairpin vortices: the counter-clockwise vortices (red) appeared on the right side of the low-speed region and the clockwise vortices (blue) appeared on the left side. A distinctive feature of the pipe flow, in comparison with the TBL flow, is that these structures grew continuously up to $y/\delta = 0.3$ and the streamwise length scale increased to 30δ, as shown in Fig. 3(b). For the TBL, however, it was shown that the streamwise spatial coherence and the organization of the structures were broken beyond the log-layer and the streamwise lengths of the very long meandering motions were 18δ–20δ.[2,4,5,34] Far from the wall ($y/\delta = 0.5$) in Fig. 3(c), the very long patterns of the structures and Reynolds shear stresses observed at $y/\delta = 0.3$ became less organized, while the spanwise extents of the low-speed motions grew. However, the previous hot-wire experimental visualization of Monty *et al.*[10] with Taylor's hypothesis showed that the very long large-scale structures persist at least until $y/\delta = 0.56$ in internal channel flow at $Re_\tau = 3178$. Since the previous measurements conducted in pipe flow by Bailey and Smits[35] found that the shape and size of the VLSM are relatively insensitive to the Reynolds number (from $Re_D = 3.1 \times 10^4$ to 3.5×10^7), such difference with the experimental data might be due to either the artificial effect induced by Taylor's field or the fundamental difference between pipe and channel flows.

These discrepancies between pipe and boundary layer flows are due to intermittency in the outer part of TBL. The effects of intermittency on the TBL flow were examined by calculating the intermittency coefficient γ, which indicates the fraction of time for which the flow is rotational at a given location.[36] In a fully turbulent flow, the vorticity is expected to be non-zero, and thus irrotational regions occur at positions at which the vorticity vanishes. Note that the vorticity magnitude $|\omega|$ can be easily computed in simulations. By contrast, intermittency measurements in experimental studies are more difficult.[29,37] Figure 5 shows the intermittency coefficient γ, computed using $|\omega|$ with a detection threshold of $|\omega|^+ = |\omega/\nu/{u_\tau}^2 = 0.0165$. The boundary layer data from Lee and Sung[5] agreed well with the data presented by Jiménez *et al.*[38] over the entire wall-normal distance. The discrepancies in the two sets of experiments were due to the use of different Reynolds numbers and identification techniques. A small fraction of the irrotational flow in the TBL was present even in

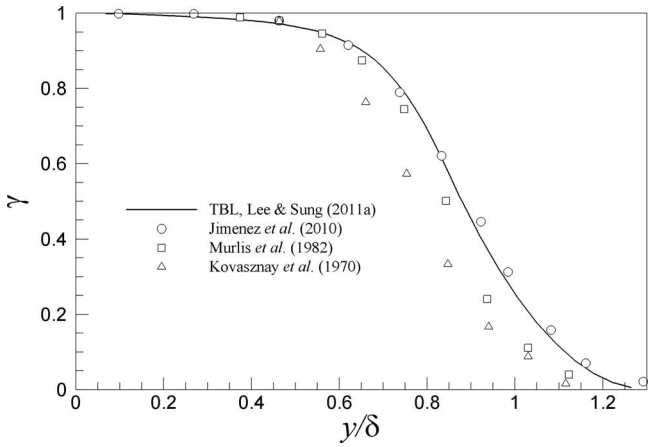

FIG. 5. Intermittency coefficient γ in the boundary layer flow.

the logarithmic layer, and the potential flow became significant for $y/\delta \geq 0.5$. Above the boundary layer δ, rotational flow with vortical structures was observed, and the influence of the rotational flow penetrated to a depth of approximately $y/\delta = 1.3$. An example of the behavior in the TBL is evidently shown in the instantaneous contour plot of $|\omega|$ in Fig. 6(a). Grey and white contours indicate the rotational and irrotational regions, respectively. As seen, large plumes of the intermittent potential flow in the outer part of the TBL were entrained into the wall-bounded layer, and the entrainment of the flow often extended to the logarithmic layer. Such penetration of the irrotational fluid induced a breakdown of the streamwise coherence created by the continuous alignment of the vortical structures above the log layer. However, in the pipe flow the entrainment was not observed (Fig. 6(b)), and the irrotational flows were locally observed throughout the wall layer. Reduced coherence among the structures in the TBL may, therefore, result from the entrainment of the potential flow by intermittency.

Another important aspect of the pipe flow, relative to the TBL flow, as shown in Figs. 3 and 4, is that the strengths of the signed swirling and the Reynolds shear stress varied. The variations in strength were examined by computing probability density functions (pdfs), and the results are shown in Figs. 7 and 8. However, since there should be noted a crucial consideration in normalizing Λ_{ci},[39] we have instead employed the wall-normal vorticity fluctuations normalized by the mean shear to

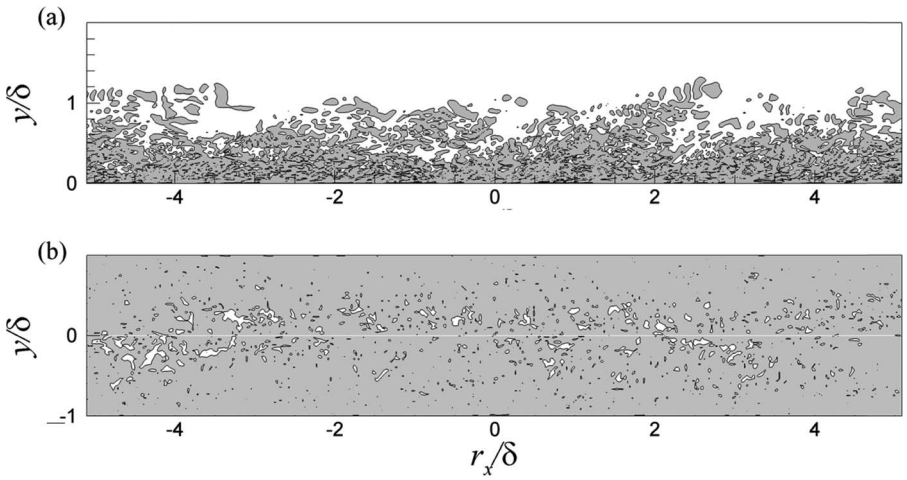

FIG. 6. Contour of the vorticity magnitude $|\omega|$ in the (a) boundary layer and (b) pipe flows. The contour level employed here is $|\omega|^+ = |\omega/\nu/{u_\tau}^2 = 0.0165$.

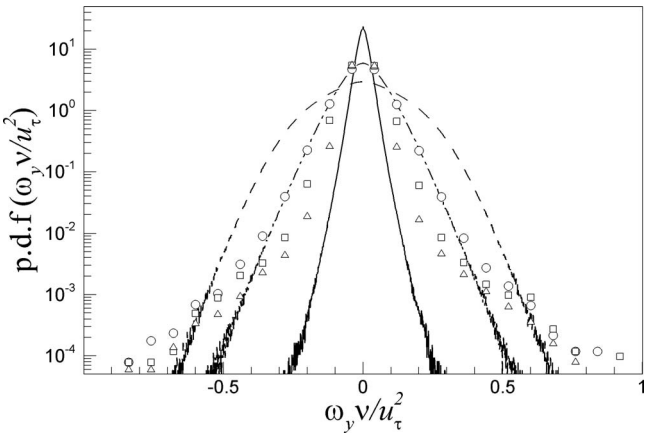

FIG. 7. Probability density functions of the wall-normal vorticity fluctuations $\omega_y \nu/{u_\tau}^2$. The black solid, dashed, and dotted lines depict the present pipe data at $y/\delta = 0.15$, 0.3, and 0.5, and the circles, squares, and triangles indicate the TBL data of Lee and Sung[5] at the same wall-normal heights, respectively.

compare the magnitude of the swirl. Although a strong swirl introduces highly elongated regions of momentum deficit,[2,34] the strong swirl motions did not necessarily indicate a long streamwise coherence in the structures, because strong swirling motions related to hairpin leg components occurred more frequently in TBL than in pipe flows. This finding supports our conclusion that the intermittency in the TBL played a more important role in the formation of very long coherent structures than was suggested by the hairpin packet model. In each flow such as TBL and pipe, however, the strength of the swirl was strongly correlated with the streamwise extent of the structures, as shown in Figs. 3 and 4. The strength of the swirl in the pipe flow increased to $y/\delta = 0.3$, then decreased above that layer. By contrast, the strength of the swirl in the TBL flow continuously decreased, similar to the streamwise coherence of the structures. Note that the pdfs were symmetric and centered at zero, indicating that the pdfs of the clockwise and counter-clockwise vortices were similar.

The pdfs in Fig. 8 show the distribution of large Q2 and Q4 Reynolds shear stresses normalized by the friction velocity in the TBL. The stronger tail for the Q4 event was particularly evident in the TBL, compared to that of the pipe flow. The strengths of the Q2 ejections were larger than those of the Q4 sweeps in both flows. Note that normalization by the local mean Reynolds shear stress yielded larger values for the Q2 and Q4 events in the pipe flow than in the TBL, although not shown here. This result indicated that the relative contributions of the Q2 and Q4 Reynolds shear stresses to the local mean Reynolds shear stress were higher in the pipe flow, whereas the magnitude of the individual quadrant components was reduced. The higher Reynolds shear stress in the TBL was attributed to the strong contributions of the irrotational fluid flow. The irrotational flow entering

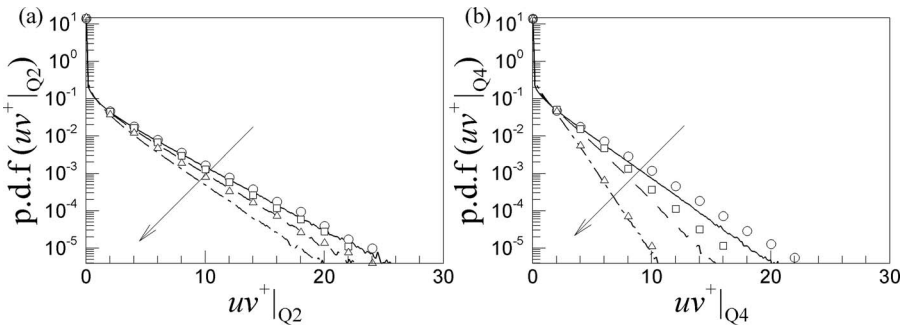

FIG. 8. The probability density functions for the (a) Q2 and (b) Q4 Reynolds shear stresses normalized by the friction velocity. The legend is the same as in Fig. 7.

the shear layer increased the momentum of the free stream in the TBL[38] but not in the pipe flow. As the wall-normal height increased, the ejections and sweeps over both flows weakened, and the imbalance between the Q2 and Q4 events increased.

Careful inspection of the high-momentum regions in Fig. 4 shows that the very long high-momentum regions were flanked by low-momentum regions in the spanwise direction and were created by alignment among the hairpin vortices. One obvious difference between the high- and low-momentum regions was in the length scale that the high-speed region was shorter than the low-speed region along the streamwise direction. These results agreed with a recent experimental study of large-scale 3D structures in a TBL by Dennis and Nickels.[7] They showed that high-speed structures tended to be shorter, although the length distributions of the high- and low-speed structures were generally similar. Asymmetric momentum regions may be created if asymmetric hairpin vortices exist in the spanwise direction with different strength of swirling for the leg or neck components. However, this explanation is contrary to our earlier finding that the pdfs of the swirling motions are almost symmetric. Because high-momentum regions are not associated with hairpin head components (strictly, retrograde vortices), the induction of high-momentum regions is weaker than that of low-momentum regions, resulting in less streamwise coherence and more irregularly shaped high-momentum regions. Note that the number of prograde vortices related to the low-momentum regions was approximately three times larger than the number of retrograde vortices.[39] The behavior observed in the instantaneous fields is examined by statistical analysis, which will be presented in Sec. V.

V. TWO-POINT CORRELATIONS OF THE VELOCITY FLUCTUATIONS

The average structural characteristics via the two-point correlations of the streamwise velocity fluctuations along the wall-normal direction were examined to support our observations found in the previous instantaneous fields, compared with those of the TBL. In addition, since there is ongoing debate for the existence of the secondary peak in the premultiplied energy spectra[18–20] and the previous comparison of the streamwise length scales between internal and external flows was based on the results from the secondary peak,[13–15,17] it is valuable to analyze the mean streamwise length scale based on the two-point correlations, as similar to those in TBLs.[5,34,40,41] To our knowledge, an analysis of the streamwise length scales based on streamwise two-point correlations has not been attempted in pipe flows because the lengths of the VLSMs have significantly exceeded the PIV (particle image velocimetry) field of view and small numerical domains. The two-point correlation coefficient is defined as

$$R_{uu}(\mathbf{r}) = \frac{\langle u(\mathbf{x})u(\mathbf{x}+\mathbf{r})\rangle}{\sqrt{\overline{u^2}}\sqrt{\overline{u^2}}}, \tag{5.1}$$

where $\boldsymbol{r}$ denotes the spatial separation and the overbar is the temporal and spatial averaged quantity.

Figures 9 and 10 show 2D views of R_{uu} in the xz and yz planes, for clarity. A long streamwise coherence with anti-correlated behavior was present due to the spanwise-adjacent low- and high-momentum regions with spanwise periodicity. In Figs. 10(a) and 10(b), the positive correlation contours in the logarithmic layer are shown to be attached to the wall. There was no correlation with the outer region, indicating that although the VLSMs in the logarithmic layer maintained a footprint on the bottom wall by modulation of the near-wall cycle in the presence of counter-rotating streamwise vortex pairs along the spanwise direction,[42] the log region structures interacted very little, in an averaged sense, with the structures in the pipe core region. As the reference height increased, the positive correlation contours were observed to be detached from the wall and the anti-correlated region gradually moved from both sides in the spanwise direction to the top side, thereby forming a roof, as shown in Fig. 10(h). The wall-normal separating distance between the positive and negative correlations in Fig. 10(h) appeared to be similar to that of the anti-correlated region in the spanwise direction ($\Delta z \approx 0.5\delta$). These features in the pipe flow are expected, because the spanwise extent ($z = r\theta$) is decreased with increasing the wall-normal height, and thus it leads to merging of the anti-correlated regions on both sides, as shown in Fig. 10(e). With continuous increase of the reference height, the merging of the negative correlations progresses further, and the

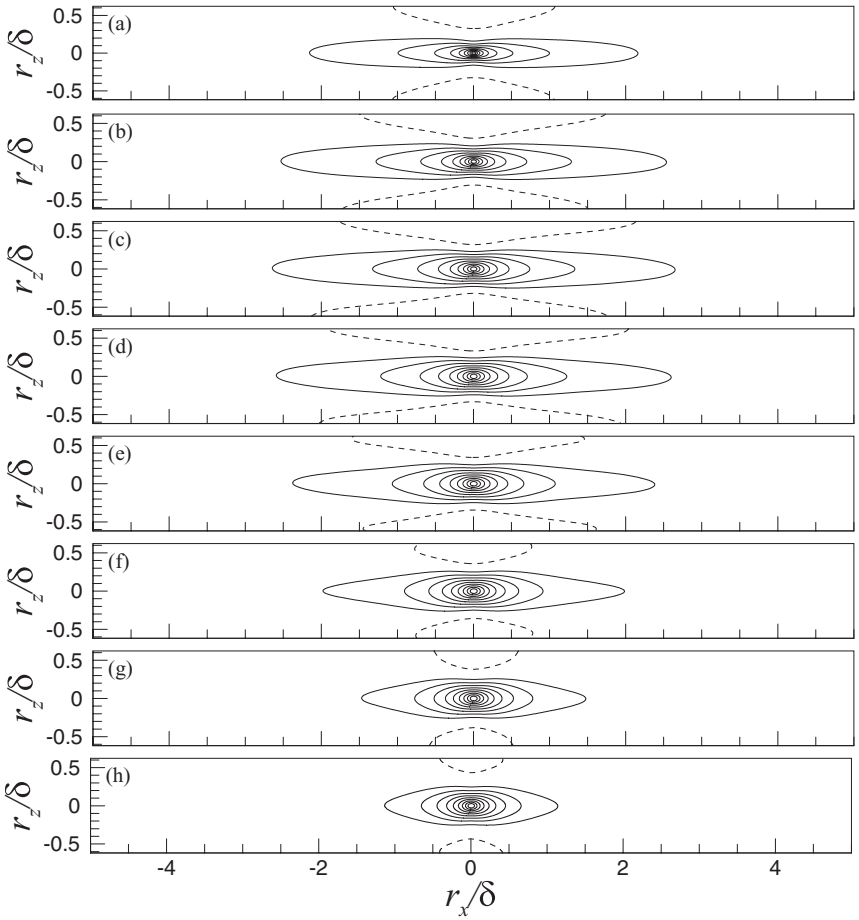

FIG. 9. Spatial correlations of the streamwise velocity fluctuations in the streamwise/spanwise planes at several wall-normal heights: (a) $y/\delta = 0.1$, (b) $y/\delta = 0.2$, (c) $y/\delta = 0.3$, (d) $y/\delta = 0.4$, (e) $y/\delta = 0.5$, (f) $y/\delta = 0.6$, (g) $y/\delta = 0.7$, and (h) $y/\delta = 0.8$. The contour levels were varied from 0.1 to 1.0 with a negative value of -0.05.

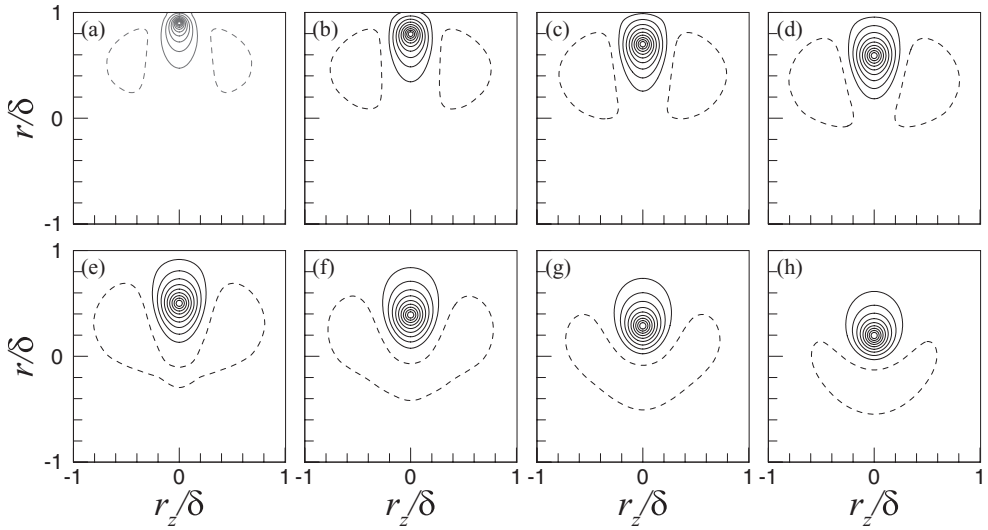

FIG. 10. Spatial correlations among the streamwise velocity fluctuations in the spanwise/wall-normal plane in the turbulent pipe flow: (a) $y/\delta = 0.1$, (b) $y/\delta = 0.2$, (c) $y/\delta = 0.3$, (d) $y/\delta = 0.4$, (e) $y/\delta = 0.5$, (f) $y/\delta = 0.6$, (g) $y/\delta = 0.7$, and (h) $y/\delta = 0.8$. The contour levels are the same as those described in Fig. 9.

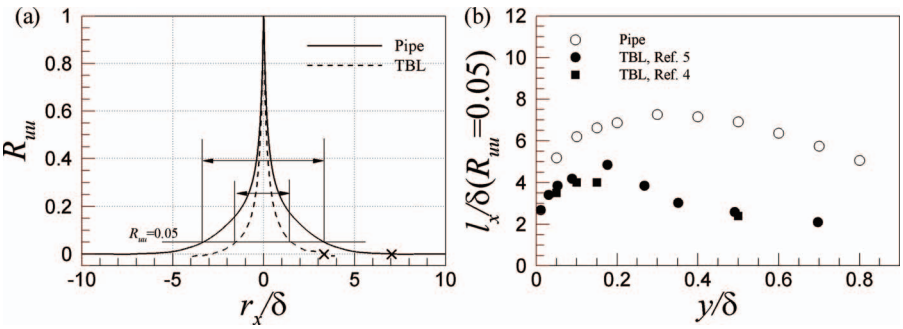

FIG. 11. (a) Streamwise line plot of R_{uu} at $y/\delta = 0.15$ with $r_z/\delta = 0$ and (b) variation of the characteristic streamwise length scale based on the range of streamwise displacement where $R_{uu} > 0.05$.

anti-signed correlated region is only visible on the top side. Note that this anti-correlated region penetrates to the opposite side of the pipe flow. This is different from the previous experimental study of Bailey and Smits[35] at which the interaction between the motions on the opposite sides was minimal.

Figure 11(a) shows streamwise line plot of R_{uu} with the reference height of $y/\delta = 0.15$ at $r_z/\delta = 0$. To compare the pipe flow behavior with that of the TBL flow, the streamwise length, based on $R_{uu} > 0.05$, is plotted in Fig. 11(b) along the wall-normal height. In (b), open circle indicates the present data, and closed circle and square denote the TBL data reported in Refs. 4 and 5. As with the TBL flow, the streamwise length of the pipe flow increased linearly inside the log region. However, while the streamwise length of the TBL flow dropped rapidly above the outer edge of the log region, the streamwise length of the pipe flow continuously increased along the wall-normal direction. Note that beyond the log layer the increasing rate in the pipe flow was gradually reduced, but it maintained a positive value up to $y/\delta = 0.3$–0.4, resulting in a maximum at that height. As moved far from the wall, the increasing rate became negative and the streamwise extent of the pipe flow reached approximately 4 pipe radii near the pipe center. At all wall-normal heights, the streamwise length scale of the correlation was larger in the pipe flow than in the TBL flow. The discrepancies increased as the wall-normal distance increased to $y/\delta = 0.5$ at which the outer region structure was more than three times longer than in the TBL. It is interesting to note that the wall-normal range at which the difference of the streamwise length scale is maximum was similar to the locations that the maximum differences of inner-scaled turbulence intensity occurred, as shown in Fig. 2(a). However, the scaled streamwise turbulence intensity in the TBL was higher in the outer region, although long structures with greater population were observed in the pipe flow. This was due to the fact that both the production and the pressures were greater in the TBL due to the intermittency than in the internal flow.[38]

In Fig. 11(a), one-dimensional correlation profile in the logarithmic layer of the pipe flow crossed from positive to negative values at the streamwise location of approximately 7δ, as depicted by $\times$ symbol. In the TBL, Hutchins and Marusic[4] showed that the correlation becomes negative at $\Delta x/\delta = 3$–3.5 in the log region and twice of this value is very similar to the length scale $O(6\delta)$ derived from an outer peak based on the energy spectrum $k_x\Phi_{uu}$. In agreement with these results, the statistical flow structure with lengths of 14δ in the pipe flow fully occupies the streamwise domain, and the location for the secondary peak on the premultiplied spectra might be $\lambda_x/\delta = 14$ ($k_x \approx 0.45$) in the log layer, if the secondary peak indeed emerges at a higher Reynolds number. Although not shown here, it is worth mentioning that our premultiplied spectra showed the absence of the secondary peak, consistent with the numerical study of del Álamo and Jiménez[18] without Taylor's hypothesis.

Figure 12(a) shows the spanwise plot line of R_{uu} at $y/\delta = 0.15$ with $r_x/\delta = 0$ and the variation in the characteristic spanwise length scale based on the streamwise two-point correlation $R_{uu} > 0.05$ is shown in Fig. 12(b). For comparison, previously reported experimental and numerical data corresponding to pipe, channel, and TBL flows have been adapted from Monty *et al.*[10] and Bailey

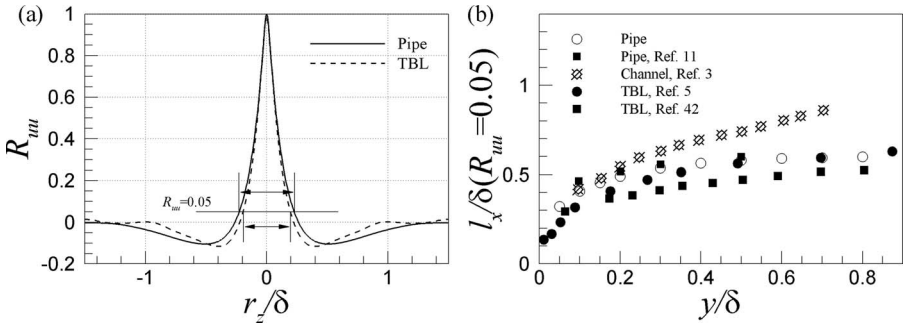

FIG. 12. (a) Spanwise line plot of R_{uu} at $y/\delta = 0.15$ with $r_x/\delta = 0$ and (b) variation of the characteristic spanwise length scale based on the range of spanwise displacement where $R_{uu} > 0.05$.

et al.[11] Note that the spanwise average length scale was extracted based on the arc length $z = r\theta$, as mentioned earlier. Although the spanwise length in both flows varied linearly in the near-wall and log regions, the spanwise extent was shown to be slightly larger in the pipe flow. Above the logarithmic layer, the structures of the pipe flow grew at a lower rate than those of the TBL flow and as a result, the spanwise length of the TBL exceeded the spanwise length of the pipe flow at approximately $y/\delta = 0.7$. Such a short spanwise length scale in the pipe core is expected because the geometry of a pipe necessarily confines the spanwise length far from the wall. This finding is consistent with previous hot-wire measurements reported by Bailey *et al*.,[11] although their measurements were limited to $y/\delta = 0.5$.

Most researchers agree that pipe and channel flows are similar because the curvature of a pipe wall is approximately zero close to the surface.[17,30] Monty *et al*.[17] found no obvious or significant differences in the spectral representations of the pipe and channel flows, even in the core region. In the present study, however, the spanwise length of structures in the pipe flow behaved differently from the spanwise length of structures in the channel flow. Note that in the absence of published channel data describing the streamwise lengths based on correlation analysis, we compared the spanwise lengths from the correlations here. Although the behavior of the spanwise length scale is similar within the log layer, it was begun to observe the large discrepancies between the pipe and channel flows far from the wall. The structure in the channel flow was shown to have the rapid increasing rate with almost constant slope up to the centerline, whereas it is not for the pipe flow. The results indicate that the coherent structures in the channel flow persisted well beyond the log layer, and therefore these structures grew continuously along the channel centerline. Further evidence supporting the present results was evident in the mean velocity profiles,[10,30] in which the profile of the channel flow extended to the outer layer lying closer to the log law than was observed in the pipe or TBL flows. This profile indicated extended coherence in channel flow structures far from the wall.

Finally, previous analysis of instantaneous flow fields, as shown in Figs. 3 and 4, showed that the high-speed long structures had shorter length scales along the streamwise direction. These properties were next examined statistically. The streamwise lengths relating to long motions may be identified by calculating the conditional two-point correlations of the streamwise velocity fluctuations. The conditional correlations are defined as

$$R_{uu}(\mathbf{r} \mid u(\mathbf{x}) > 0) = \frac{\langle u(\mathbf{x})u(\mathbf{x}+\mathbf{r}) \mid u(\mathbf{x}) > 0\rangle}{\langle u(\mathbf{x})u(\mathbf{x}) \mid u(\mathbf{x}) > 0\rangle} \quad \text{for high-speed streaks,} \tag{5.2}$$

$$R_{uu}(\mathbf{r} \mid u(\mathbf{x}) < 0) = \frac{\langle u(\mathbf{x})u(\mathbf{x}+\mathbf{r}) \mid u(\mathbf{x}) < 0\rangle}{\langle u(\mathbf{x})u(\mathbf{x}) \mid u(\mathbf{x}) < 0\rangle} \quad \text{for low-speed streaks.} \tag{5.3}$$

The resulting 2D two-point correlations for conditioned positive and negative events at $y/\delta = 0.1$, 0.3, 0.5, and 0.7 are displayed in Fig. 13. The most obvious feature of these correlations is that the positive fluctuations were biased in the upstream direction, whereas the negative fluctuations were biased in the downstream direction. The biased behavior along the streamwise direction may have

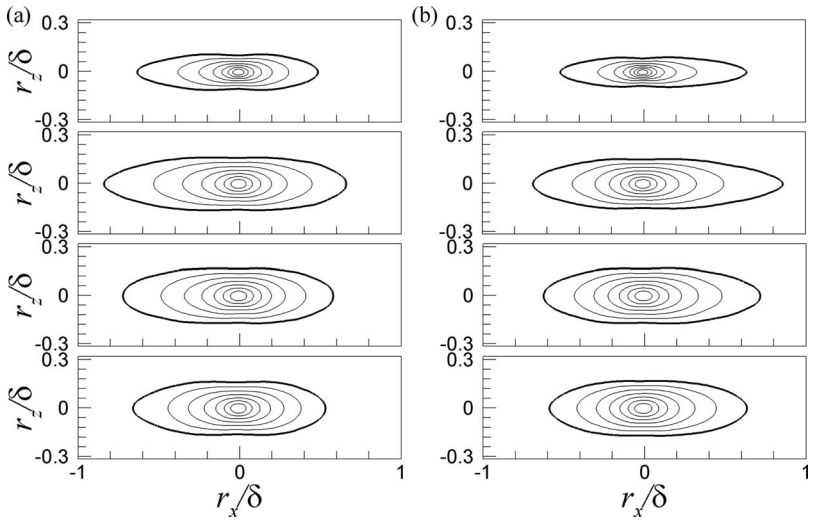

FIG. 13. Conditional two-point correlations of the streamwise velocity fluctuations at $y/\delta = 0.1$, 0.3, 0.5, and 0.7 (top to bottom) for the pipe flow. (a) $u > 0$ and (b) $u < 0$. The contour levels are varied from 0.3 to 1.0 with interval of 0.1.

resulted from the strong Q4 events (positive fluctuations) upstream of inclined packet and the Q2 events downstream of the packet. However, since the angle of inclination of the hairpin vortices in the packet increasingly changes to 90° towards the head of hairpin with the wall-normal distance from the wall, the streamwise asymmetry of the correlations becomes weaker far from the wall.

Another feature of the correlations is that the streamwise and spanwise length scales varied with the conditions of the positive and negative events, respectively. Such behavior was demonstrated by plotting the wall-normal variations of the conditional events, as shown in Fig. 14. The streamwise and spanwise length scales with no events are plotted as solid lines, for reference purposes. Because the statistics did not fully converge due to an insufficient number of conditional events, a higher threshold of $R_{uu} > 0.3$ was employed to prevent erroneous results associated with non-convergence. Consistent with the instantaneous fields, the negative structures had slightly longer streamwise length scales than the positive structures along the wall-normal distance,[41] probably due to the induction of hairpin head components. A streamwise decrease in the structures associated with conditional positive events was compensated by an increase in the spanwise length scale, as shown in Fig. 14(b). The population of the hairpin heads that contributed to the positive streamwise fluctuations (retrograde vortices) was much lower than the population of the negative fluctuations (prograde vortices), creating the weaker induction of the positive momentum region along the streamwise direction. Therefore, the structures of the positive fluctuations dispersed along the spanwise direction. Because the original two-point

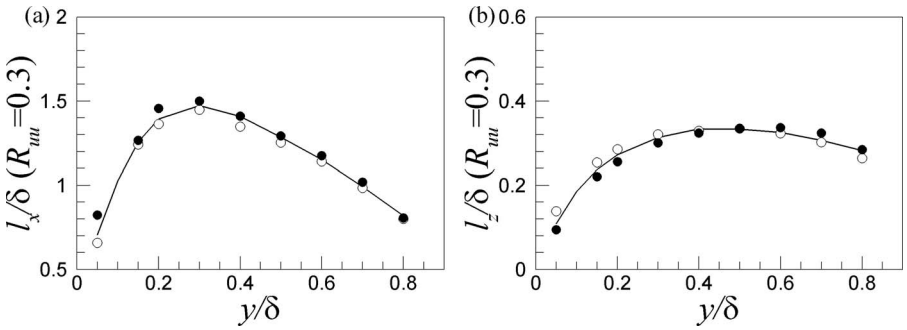

FIG. 14. Variations in the characteristic (a) streamwise and (b) spanwise length scales based on the range of streamwise and spanwise displacements where $R_{uu} > 0.3$. Open and closed circles indicate the data of conditioned events $u > 0$ and $u < 0$, respectively. For reference, the data from the two-point correlation by the definition in (5.1) is indicated by solid line.

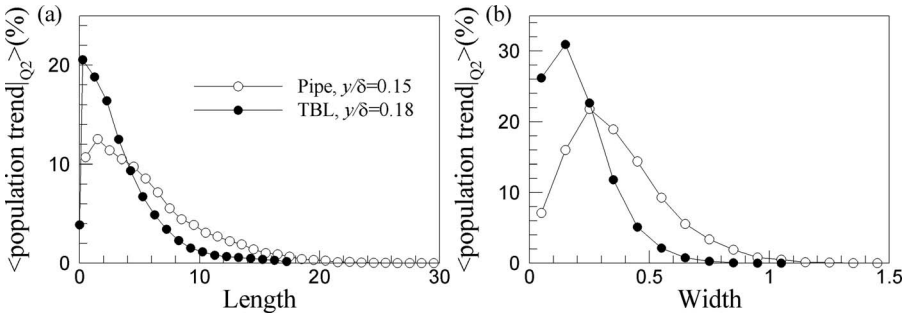

FIG. 15. Comparison of the population trends for (a) the streamwise length and (b) the spanwise width in the pipe and boundary layer flows in the logarithmic layer. The conditional events were the negative streamwise fluctuations ($u < 0$).

correlations included contributions from the positive and negative events over a wide range of length scales, the length scale containing both events is expected to be positioned between the positive and negative conditions.

VI. POPULATION TRENDS IN THE MOMENTUM REGIONS

A statistical analysis of the two-point correlations showed an increase in the streamwise and spanwise extents in the pipe flow. The question remains as to which length scales contribute most significantly to an increase in the length scales because the two-point correlations include contributions from motions over a wide range of scales. To address this question, we examined the population trends in the high- and low-momentum regions with strong Reynolds shear stress and swirling strength.[5] Figure 15 shows the length distributions of the structures identified in the logarithmic layer. The ordinates are the ratio of the number of the patches found in each length to the total number of detected patches. Note that the lengths of the VLSMs were defined as greater than 3δ in the present study, based on the criteria of Guala *et al.*[14] and Balakumar and Adrian.[15] The boundary layer data showed that the peak occurred below approximately 0.25δ (150 in wall units), showing the predominant presence of a single hairpin vortex.[2,5] In the pipe flow, however, most of the population was observed at 1δ–2δ. Because the average streamwise spacing of the hairpin vortices is on the order of ~200 in the wall units,[1,33] it was suggested that the streamwise length at which the maximum occurred was formed by successive alignment of the hairpin vortices along the streamwise direction. Note that Bailey and Smits[35] suggested that the streamwise length scale of the LSM was 1δ–2δ, based on cross-correlations using a spectral filter. In the pipe flow, the VLSMs exceeding the streamwise length 3δ accounted for more than 65% of all patches identified by the extraction scheme. The maximum length of these very long meandering negative streamwise velocity fluctuations approached $\sim 30\delta$, although the number of VLSMs was significantly reduced at longer lengths. This observation was distinguishable to the TBL flow at which the percentage of VLSMs larger than 3δ was about 40% and the largest length scale of the structures was $\sim 18\delta$.

The width distributions in the pipe and TBL flows are shown in Fig. 15(b). As with the streamwise length, the width population peak occurred at 0.2δ–0.3δ, in contrast with the width population peak in the TBL at 0.1δ–0.2δ (60–115 in wall units) in the logarithmic layer. The peak in the TBL was thought to result from the legs of predominant single hairpin vortices, because the mean spanwise width of the hairpins was 50–100 wall units.[1] A much larger spanwise width indicated that the mean width of a hairpin increased with the pipe flow. Although not shown here, inspection of the two-point correlations of the signed swirling strength supported this finding that the spanwise width of the positive peaks and negative peaks occurred at 0.2δ–0.3δ. In contrast with the streamwise length, no signs of a long tail were observed along the spanwise direction. However, the maximum width of the structures was extended to approximately 1.5δ which is 1.5 times larger than the maximum width of the structures in the boundary layer. It is noted that the factor of 1.5 is slightly different with the value of 1.25 based on the spanwise two-point correlations before due to the imperfectness of our algorithm. In conclusion, the increase in the streamwise length and spanwise width appeared to be

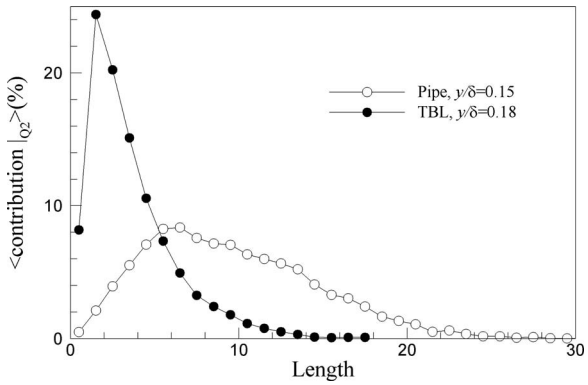

FIG. 16. Contribution to the total second-quadrant Reynolds shear stress identified by the feature extraction algorithm as a function of the length for both the pipe and boundary layer flows in the logarithmic layer. The length is normalized by the outer unit.

due to both the large population of long and wide structures and to an increase in the maximum lengths and widths of the structures.

The length contributions to the total Reynolds shear stress are shown in Fig. 16. The values were computed according to the ratio of the total second-quadrant Reynolds shear stress associated with all patches included in a certain length to the sum of the second-quadrant Reynolds shear stress for all patches identified by the feature extraction algorithm. The maximum contribution to the Reynolds shear stress in the TBL flow arose at 1δ–2δ in the log region due to the streamwise-aligned hairpin packets.[2,5] In the present pipe flow, the peak of the contribution for the Reynolds shear stress occurred at approximately 6δ, whereas the population peak in Fig. 16(a) was observed at 1δ–2δ, indicating a higher contribution of the VLSMs to the Reynolds shear stress in pipe flow than in TBL flow. When the total Reynolds shear stress identified by the extraction algorithm was divided by the global sum of all Reynolds shear stresses in all vector fields, we found that the contribution of the log layer was more than 30%, consistent with previous findings based on an analysis of the cumulative energy spectrum.

VII. SUMMARY AND CONCLUSIONS

We conducted a DNS of a turbulent pipe flow to investigate the spatial features and properties of its VLSMs in comparison to TBL flows. The DNS results with first- and second-order statistics were validated with the previous pipe DNS data, and showed good agreement. The comparison of the profiles for mean velocity between the pipe and TBL flows showed that although the mean velocity of the TBL far from the wall exceeded that of the pipe flow due to the high momentum in the potential region, the logarithmic mean velocity in the TBL was somewhat smaller than in the pipe flow. In agreement with previous findings, it was found that the fluctuations of the transverse velocity and Reynolds shear stress were stronger in the TBL than in the pipe. However, although most studies had previously concluded that the streamwise velocity fluctuations for internal and external flows were similar, we found that the streamwise velocity fluctuations were higher in the TBL, and maximum differences were observed at $y/\delta = 0.3$–0.6, consistent with that of Jiménez *et al.*[38]

In the present pipe flow, the large- and very-large-scale structures were present both in the logarithmic layer and wake regions, and these motions were closely associated with a strong swirling strength and Reynolds shear stress. Because the high-momentum regions were not closely related to the hairpin head components, the very long high-momentum regions yielded slightly shorter streamwise length scales than were observed in the low-momentum regions. On the other hand, a distinctive feature of the pipe flows, relative to the TBL flows, was that these structures grew continuously to $y/\delta = 0.3$–0.4 and yielded a maximum streamwise length of 30δ. The streamwise spatial organization of structures in the TBL flow was broken beyond the log-layer, and the streamwise lengths of the

VLSMs were approximately 18δ. These structural discrepancies arose from the different natures that contributed to the irrotational flows in the shear layers. In TBL flows, large plumes of intermittent potential flows in the outer regions entrained into the wall-bounded layer and often extended to the logarithmic layer. The large plumes then induced breakdown of the streamwise coherence of the structures above the log layer and enhanced the strength of the swirling motions and Reynolds shear stress. In the pipe flow, such entrainment was not observed, and the irrotational regions occurred intermittently or locally throughout the wall layer.

Contrary to the two-point correlation coefficient of the streamwise velocity fluctuations in the TBL, the correlation contours in the wake region of the pipe flow were shown to emerge the anti-correlated region from both sides in the spanwise direction to the top side with increasing the wall-normal distance from the wall, indicating the interaction between the motions on the opposite sides in the pipe flow. In addition, the streamwise length scale of the correlation was larger in the pipe flow than in the TBL flow at all wall-normal heights and the maximum discrepancy was observed at $y/\delta = 0.5$ at which the outer region structure was more than three times longer than in the TBL. However, the difference of the spanwise length scales between the pipe and boundary layer flows was not significant, compared to the streamwise length scale, and the maximum difference was 1.25 times wider in the log layer. Moreover, since the structures in the pipe flow grew at the lower increasing rate than those of the TBL flow beyond the log layer, the spanwise length scale of the TBL became similar to that in the pipe flow in the outer layer. The analysis of the streamwise energy spectra using our pipe DNS data showed that there was no dominant peak at long wavelength associated with the VLSMs. However, one-dimensional correlation profile in the log layer of the pipe flow crossed over from positive to negative values at streamwise separation of $\sim 7\delta$. This result indicated that if the secondary peak in the streamwise energy spectra might occur at a higher Reynolds number, the wavenumber for the secondary peak might be approximately $k_x \approx 0.45$ with wavelength of $\lambda_x/\delta = 14$.

The populations of the momentum regions with strong Reynolds shear stress and swirling strength were estimated to give answer as to which length scales contribute most significantly to the increase in the length scales in the pipe flow. The results showed that the longer length scales arose from a large population of long structures ($>3\delta$) and the longer maximum lengths of the structures in the pipe flow. Additionally, when the total Reynolds shear stress identified by the extraction algorithm was divided by the global sum of all Reynolds shear stresses in all vector fields, the contribution of the log layer exceeded 30%.

ACKNOWLEDGMENTS

This work was supported by the Creative Research Initiatives (No. 2012-0000246) program of the National Research Foundation and was partially supported by KISTI under the Strategic Supercomputing Support Program.

[1] R. J. Adrian, C. D. Meinhart, and C. D. Tomkins, "Vortex organization in the outer region of the turbulent boundary layer," J. Fluid Mech. **422**, 1 (2000).
[2] B. Ganapathisubramani, E. K. Longmire, and I. Marusic, "Characteristics of vortex packets in turbulent boundary layers," J. Fluid Mech. **478**, 35 (2003).
[3] J. C. del Álamo, J. Jiménez, P. Zandonade, and R. D. Moser, "Scaling of the energy spectra of turbulent channels," J. Fluid Mech. **500**, 135 (2004).
[4] N. Hutchins and I. Marusic, "Evidence of very long meandering features in the logarithmic region of turbulent boundary layers," J. Fluid Mech. **579**, 1 (2007).
[5] J. H. Lee and H. J. Sung, "Very-large-scale motions in a turbulent boundary layer," J. Fluid Mech. **673**, 80 (2011).
[6] D. J. C. Dennis and T. B. Nickels, "Experimental measurement of large-scale three-dimensional structures in a turbulent boundary layer. Part 1. Vortex packets," J. Fluid Mech. **673**, 180 (2011).
[7] D. J. C. Dennis and T. B. Nickels, "Experimental measurement of large-scale three-dimensional structures in a turbulent boundary layer. Part 2. Long structures," J. Fluid Mech. **673**, 218 (2011).
[8] R. J. Adrian, "Hairpin vortex organization in wall turbulence," Phys. Fluids **19**, 041301 (2007).
[9] I. Marusic, B. J. Mckeon, P. A. Monkewitz, H. M. Nagib, A. J. Smits, and K. R. Sreenivasan, "Wall-bounded turbulent flows at high Reynolds numbers: Recent advances and key issues," Phys. Fluids **22**, 065103 (2010).
[10] J. P. Monty, J. A. Stewart, R. C. Williams, and M. S. Chong, "Large-scale features in turbulent pipe and channel flows," J. Fluid Mech. **589**, 147 (2007).

[11] S. C. C. Bailey, M. Hultmark, A. J. Smits, and M. P. Schultz, "Azimuthal structure of turbulence in high Reynolds number pipe flow," J. Fluid Mech. **615**, 121 (2008).
[12] D. J. C. Dennis and T. B. Nickels, "On the limitations of Taylor's hypothesis in constructing long structures in a turbulent boundary layer," J. Fluid Mech. **614**, 197 (2008).
[13] K. C. Kim and R. J. Adrian, "Very large-scale motion in the outer layer," Phys. Fluids **11**, 417 (1999).
[14] M. Guala, S. E. Hommema, and R. J. Adrian, "Large-scale and very-large-scale motions in turbulent pipe flow," J. Fluid Mech. **554**, 521 (2006).
[15] B. J. Balakumar and R. J. Adrian, "Large- and very-large-scale motions in channel and boundary-layer flows," Philos. Trans. R. Soc. London, Ser. A **365**, 665 (2007).
[16] J. Jiménez, "The largest scales of turbulent wall flows," *Center for Turbulence Research, Annual Research Briefs* (Stanford University, 1998), pp. 137–154.
[17] J. P. Monty, N. Hutchins, H. C. H. Ng, I. Marusic, and M. S. Chong, "A comparison of turbulent pipe, channel and boundary layer flows," J. Fluid Mech. **632**, 431 (2009).
[18] J. C. delÁlamo and J. Jiménez, "Estimation of turbulent convection velocities and corrections to Taylor's approximation," J. Fluid Mech. **640**, 5 (2009).
[19] X. Wu, J. R. Baltzer, and R. J. Adrian, "Direct numerical simulation of a $30R$ long turbulent pipe flow at $R^+ = 685$: Large- and very large-scale motions," J. Fluid Mech. **698**, 235 (2012).
[20] J. Kim, "Progress in pipe and channel flow turbulence, 1961–2011," J. Turbul. **13**, 1 (2012).
[21] J. H. Lee and H. J. Sung, "Direct numerical simulation of a turbulent boundary layer up to $Re_\theta = 2500$," Int. J. Heat Fluid Flow **32**, 1 (2011).
[22] K. Kim, S. J. Baek, and H. J. Sung, "An implicit velocity decoupling procedure for the incompressible Navier-Stokes equations," Int. J. Numer. Methods Fluids **38**, 125 (2002).
[23] K. Akselvoll and P. Moin, Report No. TF-63, Thermoscience Division, Department of Mechanical Engineering, Stanford University, 1995.
[24] S. J. Jang, H. J. Sung, and P. Å. Krogstad, "Effects of an axisymmetric contraction on a turbulent pipe flow," J. Fluid Mech. **687**, 376 (2011).
[25] C. Chin, A. S. H. Ooi, I. Marusic, and H. M. Blackburn, "The influence of pipe length on turbulence statistics computed from direct numerical simulation data," Phys. Fluids **22**, 115107 (2010).
[26] X. Wu and P. Moin, "A direct numerical simulation study on the mean velocity characteristics in turbulent pipe flow," J. Fluid Mech. **608**, 81 (2008).
[27] P. Schlatter and R. Örlü, "Assessment of direct numerical simulation data of turbulent boundary layers," J. Fluid Mech. **659**, 116 (2010).
[28] H. M. Nagib and K. A. Chauhan, "Variations of von Karman coefficient in canonical flows," Phys. Fluids **20**, 101518 (2008).
[29] J. Murlis, H. Tsai, and P. Bradshaw, "The structure of turbulent boundary layers at low Reynolds numbers," J. Fluid Mech. **122**, 13 (1982).
[30] H. C. H. Ng, J. P. Monty, N. Hutchins, M. S. Chong, and I. Marusic, "Comparison of turbulent channel and pipe flows with varying Reynolds number," Exp. Fluids **51**, 1261 (2011).
[31] M. Hultmark, S. C. C. Bailey, and A. J. Smits, "Scaling of near-wall turbulence in pipe flow," J. Fluid Mech. **649**, 103 (2010).
[32] L. H. O. Hellström, A. Sinha, and A. J. Smits, "Visualizing the very-large-scale motions in turbulent pipe flow," Phys. Fluids **23**, 011703 (2011).
[33] J. Zhou, R. J. Adrian, S. Balachandar, and T. M. Kendall, "Mechanisms for generating coherent packets of hairpin vortices," J. Fluid Mech. **387**, 353 (1999).
[34] C. D. Tomkins and R. J. Adrian, "Spanwise structure and scale growth in turbulent boundary layers," J. Fluid Mech. **490**, 37 (2003).
[35] S. C. C. Bailey and A. J. Smits, "Experimental investigation of the structure of large- and very-large-scale motions in turbulent pipe flow," J. Fluid Mech. **651**, 339 (2010).
[36] D. K. Bisset, J. C. R. Hunt, and M. M. Rogers, "The turbulent/non-turbulent interface bounding a far wake," J. Fluid Mech. **451**, 383 (2002).
[37] S. Corrsin and A. L. Kistler, "Free-stream boundaries of turbulent flows," Technical Report No. 1244, NACA, 1955.
[38] J. Jiménez, S. Hoyas, M. P. Simens, and Y. Mizuno, "Turbulent boundary layers and channels at moderate Reynolds numbers," J. Fluid Mech. **657**, 335 (2010).
[39] Y. Wu and K. T. Christensen, "Population trends of spanwise vortices in wall turbulence," J. Fluid Mech. **568**, 55 (2006).
[40] N. Hutchins, W. T. Hambleton, and I. Marusic, "Inclined cross-stream stereo particle image velocimetry measurements in turbulent boundary layers," J. Fluid Mech. **541**, 21 (2005).
[41] B. Ganapathisubramani, N. Hutchins, W. T. Hambleton, E. K. Longmire, and I. Marusic, "Investigation of large-scale coherence in a turbulent boundary layer using two-point correlations," J. Fluid Mech. **524**, 57 (2005).
[42] N. Hutchins and I. Marusic, "Large-scale influences in near-wall turbulence," Philos. Trans. R. Soc. London, Ser. A **365**, 647 (2007).